Journal Pre-proof

Investigations on the microwave absorption properties and thermal behavior of vanadium slag: Improvement in microwave oxidation roasting for recycling vanadium and chromium

Kangqiang Li, Qi Jiang, Lei Gao, Jin Chen, Jinhui Peng, Sivasankar Koppala, Mamdouh Omran, Guo Chen

PII: S0304-3894(20)30687-7

DOI: https://doi.org/10.1016/j.jhazmat.2020.122698

Reference: HAZMAT 122698

To appear in: *Journal of Hazardous Materials*

Received Date: 2 February 2020

Revised Date: 2 March 2020

Accepted Date: 9 April 2020

Please cite this article as: Li K, Jiang Q, Gao L, Chen J, Peng J, Koppala S, Omran M, Chen G, Investigations on the microwave absorption properties and thermal behavior of vanadium slag: Improvement in microwave oxidation roasting for recycling vanadium and chromium, *Journal of Hazardous Materials* (2020), doi: https://doi.org/10.1016/j.jhazmat.2020.122698

Investigations on the microwave absorption properties and thermal behavior of vanadium slag: Improvement in microwave oxidation roasting for recycling vanadium and chromium

Kangqiang Li [a], Qi Jiang [a], Lei Gao [b], Jin Chen [a, **], Jinhui Peng [a, b], Sivasankar Koppala [c], Mamdouh Omran [d], Guo Chen [a, b, c, *]

[a] *Key Laboratory of Unconventional Metallurgy, Ministry of Education, Kunming University of Science and Technology, Kunming 650093, P.R. China.*

[b] *Key Laboratory of Green-Chemistry Materials in University of Yunnan Province, Kunming Key Laboratory of Energy Materials Chemistry, Yunnan Minzu University, Kunming 650500, P.R. China.*

[c] *Panjin Institute of Industrial Technology, Dalian University of Technology, Panjin 124221, Liaoning, P.R. China.*

[d] *Process Metallurgy Research Group, Faculty of Technology, University of Oulu, Finland.*

* Corresponding author: guochen@kust.edu.cn

** Co-corresponding author: jinchen@kust.edu.cn

Graphical abstract

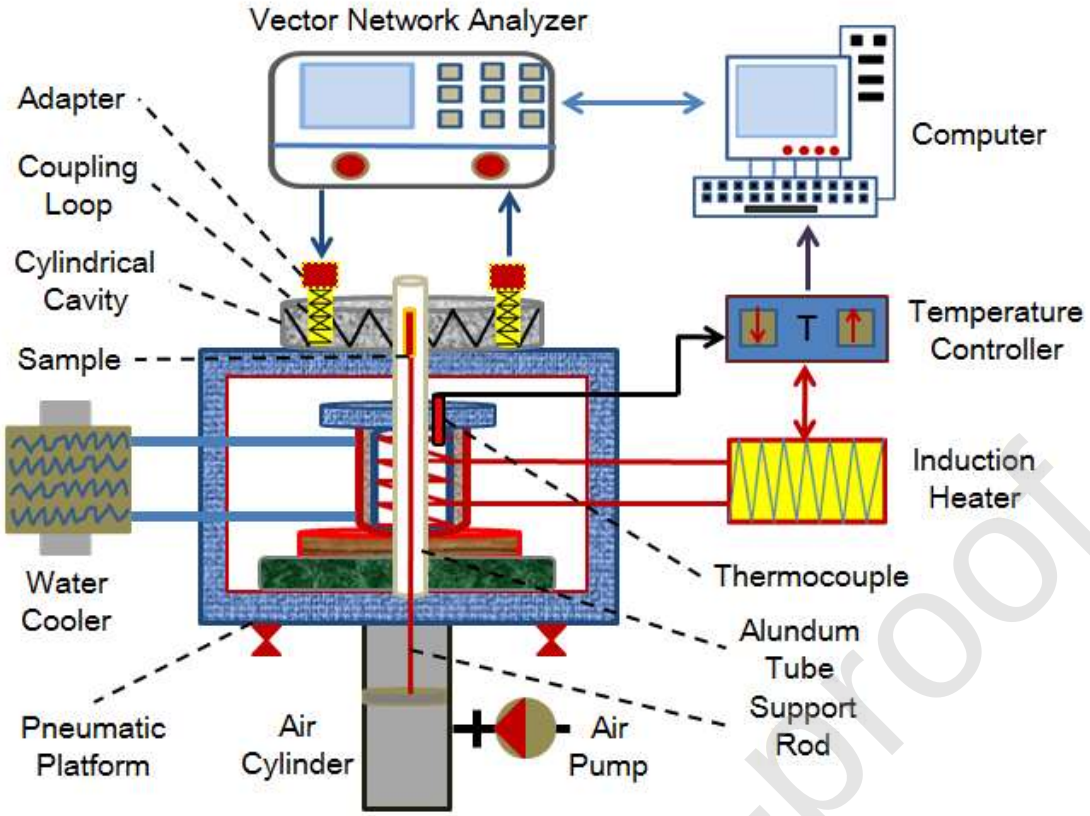

Schematic diagram of dielectric test system

Highlights

- •Determination of the microwave absorption properties of vanadium slag the first time.
- •Investigation of the thermal behavior of vanadium slag in microwave field.
- •Microwave absorption properties are closely related to the thermal behavior.
- •Declaration of the feasibility of applying microwave heating to vanadium slag.

Abstract

Vanadium slag contains high contents of vanadium and chromium with complex and dense structures, hence microwave heating instead of conventional methods is expected to

destroy the dense structure and further to improve the extraction rate of vanadium and chromium, and exploring its dielectric properties is the prerequisite work. Microwave absorption properties and thermal behavior of vanadium slag were investigated. Results indicated that vanadium slag endowed excellent microwave absorption properties, with minimum ε_r' value of 34.447 (F/M). Dielectric properties of vanadium slag varied with temperature, which changing trend was matched to the three stages of microwave heating characteristics identified by heating rates. Meanwhile, the changing process of dielectric properties also corresponded to the three processes of thermogravimetric characteristics: dehydration stage (30 °C-280 °C), oxidation decomposition of olivine phase and normal spinel phase (280 °C-650 °C), and oxidation decomposition of vanadium chromium spinel (650 °C-950 °C). Moreover, the maximum dielectric constant and highest microwave heating rate of vanadium slag both appeared at the temperature regime of 500 °C-550 °C, which was also the main temperature regime for oxidation decomposition of olivine phase and normal spinel phase in vanadium slag, demonstrating the appropriate process temperature for microwave heating technology to recycle vanadium slag.

Keywords: vanadium slag; chromium; microwave absorption properties; thermal behavior; microwave oxidation roasting

1 Introduction

Vanadium is known as the metal “vitamin”, manifesting as about 90% of vanadium is applied in the steel industry to improve the strength, toughness, and wear resistance of steel (Liu et al., 2018; Takahashi and Kawakami, 2018), and other wider applications of the

remaining 10% is reported in the production of alloys, batteries, catalysts, ceramics, photovoltaics, pigments, and glasses (Abbas et al., 2019; Oldenburg et al., 2019; Yin et al., 2019; Svoboda et al., 2018). Vanadium slag is the direct resource to extract vanadium. During the smelting process of steel, vanadium titanium magnetite is reduced into vanadium compounds and meanwhile pig iron is formed, followed by pig iron containing the enriched vanadium compounds is oxidized and the steel slag is produced, namely vanadium slag (Li and Zheng, 2019; Teng et al., 2019). With the increasingly widespread applications of high-quality vanadium steel and coupled with the expansion of new fields of vanadium applications, the demand for vanadium is increasing, accompanying with the increment of vanadium slag produced (Zhang et al., 2019). The high contents of vanadium (V) and chromium (Cr) and other valuable ingredients in vanadium slag need to be recycled, thereby reducing the inestimable loss from waste of resources and environmental harm. Currently, the sodium roasting-leaching method is the main applied method to extract vanadium from vanadium slag, achieved through one or more sodium salts are mixed with vanadium slag and then roasted to be converted into water-soluble sodium vanadate, and then leached by water dissolution; finally, vanadium pentoxide (V_2O_5) or vanadium trioxide (V_2O_3) products are prepared through processes such as impurity removal, vanadium precipitation, fused sheet, and reduction (Li and Zheng, 2019). Wang et al. reviewed that in the oxidization roasting-leaching method, the respective recovery rate of vanadium (V) and chromium (Cr) was only 75% and approximate zero after repeated roasting at a high temperature up to 850 °C, accompanying with the discharge of toxic tailings and hazardous gases (Wang et al., 2014). The conventional method for the extraction of vanadium and chromium from

vanadium slag performed low efficiency, and accompanied with high energy consumption and high treatment cost for large amount of waste water and waste gas, seriously polluting the environment and gradually becoming the bottleneck of vanadium extraction from vanadium slag (Liu and Wang, 2017; Wang et al., 2014; Wen et al, 2019). Regarding conventional methods are difficult to destroy the complex and dense structures of vanadium slag, rendering it difficult to expose hazardous elements from vanadium slag, such as vanadium (V) and chromium (Cr), further to aggravate the difficulty and pressure of subsequent processes. Hence, there exists an urgent demand for introducing some selective heating techniques to provide solutions for these technical problems related to vanadium and chromium extraction from vanadium slag.

The alternative applications of microwave heating to replace conventional heating has been frequently reported in the fiery fields, such as mineral pretreatment, material synthesis, alloys preparation, and secondary waste recycling, etc. (Cheng et al., 2018; Li et al., 2019a; Li et al., 2020a; Zhao et al., 2020). Specifically, in the secondary recycling of vanadium slag resources, Gao and Jiang highlighted that compared with conventional roasting on high-chromium vanadium slag, the heating time decreased by 16 min through microwave roasting, the roughness and porosity of the sample significantly improved, and the leaching ratio of V and Cr correspondingly improved from 12.7% and 0.4% to 95.9% and 4.2%, both much higher than that of by conventional roasting, with only 82.5% and 2.1% (Gao and Jiang, 2018). Zhang and Liu reported that referring to the effects of conventional blank roasting on high-chromium vanadium slag, microwave blank roasting can significantly improve the oxidative decomposition of olivine phase and spinel phase and accelerated the formation of

Fe_2TiO_5 phase, accompanying with smaller grains and more porous on the surface (Zhang and Liu, 2016). The advantageous performance of microwave heating is assigned to its unique heat generation and heat transferring mechanisms (Chen et al., 2018; Li et al., 2020b; Lin et al., 2019). Its mechanism refers to that the required microwave energy is directly transferred to the reaction atoms or molecules through the dielectric loss produced inside of the substance, thus rendering the advantageous performance than conventional heating, including the reduction of process temperature, operation time, energy consumption, and environment pollution (Li and Long, 2020; Li et al., 2020c; Yang et al., 2019).

The microwave absorption properties of a substance are represented by the two parts: the dielectric properties and microwave heating characteristics. Wherein the dielectric properties theoretically denote the ability of materials to absorb microwave energy and the efficiency of converting the absorbed microwave energy into thermal energy, and the microwave heating characteristics indicate the actual heating efficiency and the responsiveness of the substance to microwaves, which is mainly manifested by the heating time and the change in heating rate with temperature. Moreover, the microwave heating characteristics and the dielectric properties can both conversely verify the correctness and rationality of the other value. Additionally, the dielectric properties are mainly influenced by temperature, the magnetic field frequency, the particle size and phase composition of the measured substance, wherein the influence of temperature is especially significant. Li et al. and Ye et al. explored the microwave absorption properties of electrolytic manganese anode mud and waste hydrodesulfurization catalysts (both as hazardous materials), respectively, and highlighted that temperature significantly affected the dielectric properties and microwave heating

characteristics of materials (Li et al., 2020d; Ye at al., 2019). Therefore, before applying microwave heating technology to process a material, it is fundamental to investigate the microwave absorption properties of the material, further to render the related application of microwave heating technology more scientific and efficient. Furthermore, referring to the mechanism of microwave heating technology and the chemical compositions of vanadium slag, it could be surmised that microwave heating technology has brilliant application prospects to process vanadium slag, assigned to that various metal compounds in vanadium slag endows excellent microwave absorption properties (He et al., 2019; Li et al., 2020d).

The high contents of vanadium (V) and chromium (Cr) in vanadium slag need to be recycled to reduce the degree of waste of resources and the harm to the environment. Previous work mostly adopted the oxidization roasting-leaching method with different sodium salts or calcareous additives to extract vanadium (V) and chromium (Cr) hazardous elements from vanadium slag through conventional heating (Chen et al., 2020; Teng et al., 2019; Zhang et al., 2019; Wen et al, 2019). Meanwhile, a few recent studies have elucidated the alternative applications of microwave heating to replace conventional heating on the extraction of vanadium (V) and chromium (Cr) from vanadium slag, and highlighted the outstanding advantages of microwave heating compared with conventional heating, which enriched the application examples of microwave heating to process vanadium slag (Gao and Jiang, 2018; Tian et al., 2019; Zhang et al., 2019; Zhang and Liu, 2016). However, no report has investigated the microwave absorption properties and thermal behavior of vanadium slag during microwave oxidation roasting, rendering there lacks the fundamentally theoretical research on the feasibility of microwave applications on vanadium slag. Hence, in this work,

the microwave absorption properties of vanadium slag were explored to clarify the feasibility of applying microwave heating on vanadium slag, including the dielectric properties and microwave heating characteristics. Detailedly, the microwave heating characteristics were measured to verify the rationality and correctness of dielectric properties analysis. Additionally, the thermal behavior of vanadium slag were investigated to reveal the oxidation decomposition behavior of vanadium slag, through the analysis of thermodynamics characteristics, thermogravimetric characteristics and phase structure characterization, further contributing to explore the relationship between the microwave absorption properties and thermal behavior in the microwave field.

2 Materials and methods

2.1 Materials

Vanadium slag was treated as the research object in this study, received from Panzhihua Iron & Steel Research Institute (Panzhihua City, Sichuan province, P.R. China). The elemental compositions of vanadium slag were displayed in Table 1, which the analytical results were confirmed using X-Ray Fluorescence (ZSX PrimusⅣ, Rigaku, Japan) with the B-U_Solid_N_018 analytical method, conducting by Advanced Analysis and Measurment Center of the Yunnan University (Kunming City, Yunnan province, P.R. China). As observed from Table 1, the vanadium slag was characterized with high vanadium content (V, 7.37%) and high chromium content (Cr, 1.38%). In addition, the vanadium slag was obtained from oxidative blowing of vanadium-containing molten iron in the process of vanadium extraction; therefore, as presented in Table 1, the vanadium slag also contained a considerable content of

iron, manganese and titanium, which are worth recycling.

The XRD pattern and FT-IR spectra of the vanadium slag were displayed in Fig. 1, which the corresponding result was performed using X-Ray Diffractometer (D/max-TTRIII, Rigaku, Japan) and FT-IR Spectroscopy (iS50 FT-IR, Nicolet, USA). As provided in Fig. 1(a), the vanadium slag mainly contained (Mn, Fe)(V, Cr)$_2$O$_4$ phase (i.e. normal spinel phase, JCPDS: 35-0550) and (Mn, Fe)$_2$SiO$_4$ phase (i.e. olivine phase, JCPDS: 85-1347); besides, there also existed a minor amount of Fe$_2$TiO$_4$ phase (JCPDS: 34-0177), Fe$_2$O$_3$ phase (JCPDS: 19-0629), and SiO$_2$ phase (JCPDS: 50-1431). In addition, as depicted in Fig. 1(b), for the vanadium slag, the FT-IR absorption bands appeared at 468.09 cm^{-1}, 578.52 cm^{-1}, 876.59 cm^{-1}, 962.88 cm^{-1}, 1636.80 cm^{-1}, and 3456.70 cm^{-1}. Detailedly, the stretching and bending vibrations of -OH bond of surface water molecules in vanadium slag correspondingly cause the absorption bands at 1636.80 cm^{-1} and 3456.70 cm^{-1} (Chen et al., 2014; Mostafa et al., 2009); the rocking vibrations of Si-O-Si bond in SiO$_2$ phase and the stretching mode of Fe-O bond at the octahedral sites in (Mn, Fe)(V, Cr)$_2$O$_4$ phase result the absorption band at 468.09 cm^{-1}, which is a superimposed bond (Hoex et al., 2006), meanwhile, the stretching modes of metal-O bonds at the octahedral sites in (Mn, Fe)(V, Cr)$_2$O$_4$ phase arouse the absorption band at 578.52 cm^{-1} (Ishii and Nakahira, 1972); additionally, the asymmetric stretching vibrations of Si-O bond of [SiO$_4$] tetrahedra bands in (Mn, Fe)$_2$SiO$_4$ phase cause the narrow absorption bands at 876.59 cm^{-1} and 962.88 cm^{-1} (Jeanloz, 1980).

2.2 Instrumentation

The microwave absorption properties of a substance are represented by the two parts: the dielectric properties and microwave heating characteristics. Wherein the dielectric properties

of vanadium slag was determined using the dielectric test device (Agilent-E5071C, MYWAVE) by cylindrical cavity perturbation method, and the microwave heating characteristics of vanadium slag was measured using a microwave furnace (HM-X08-16, MAKEWAVE). The respective schematic diagram of the involved instrumentation was exhibited in Fig. 2 and Fig. 3.

As demonstrated in Fig. 2(a), the main constructions of the dielectric device included adapter and coupling loop, a cylindrical resonant cavity (TM_{0n0}), water circulation cooling apparatus attached to the temperature control system, air compressor, eddy current heating system, vector network analyzer, and electronic computer. Meanwhile, as presented in Fig. 2(b), the resonant cavity was mainly composed by microwave cavity, alundum tube, exciter, and detector. In addition, as exhibited in Fig. 3, the main constructions of the microwave furnace included magnetrons and microwave cavity, insulating brick and thermocouple, a computer control system, barometers and valves attached to the vacuum pump, and gas generator.

2.3 Procedure

The received vanadium slag was in powder form, with a particle size ranging from 80 mesh to 180 mesh, which met the sample requirements of the characterization analysis for the microwave absorption properties, thermal behavior and phase structure. Before testing, vanadium slag was dried at 105 °C for 12 h to exclude the influence of moisture on the measurement of the microwave absorption properties and thermal behavior of vanadium slag. After drying, a quartz tube with 4 mm in diameter and 40 mm in height was filled with a certain weight of dried slag sample (about 4.4 g), with the filled volume accounting about

more than four-fifths. During the filling process, the quartz tube is loading with the slag sample while vibrating at the same time until the quartz tube is densely packed, and a part of the upper end of the quartz tube is left with a small amount of thermal insulation cotton plug. Therefore, the quality of the filled sample will vary according to the type and size of the sample. After filling, the quartz tube loaded with the slag sample was subjected to the dielectric device to measure the dielectric properties, measured under the microwave frequency of 2450 MHz from room temperature to 850 °C without protective atmosphere. The dielectric properties of the substance was determined by the four test steps followed by cavity calibration, quartz empty tube calibration, charging and loading quartz tube test, and recalculation by the attached program control software (Li et al., 2019b; Li et al., 2019c). By the way, the more comprehensive related introduction about the dielectric properties was provided in Supplementary material. Additionally, 50.0 g of the dried slag sample was introduced to the microwave furnace to investigate the microwave heating characteristics, measured under the same frequency of 2450 MHz and the temperature regime of room temperature to 950 °C without protective atmosphere, and at different microwave powers (including 600 W, 800 W, 1000 W, and 1200 W). Besides, 10.0 mg of the dried slag sample was introduced to the simultaneous thermal analyzer (STA 449F3, NETZSCH, Germany) to conduct the thermogravimetric characteristics analysis, measured at different heating rates (including 10 °C/min, 20 °C/min, and 30 °C/min) and the temperature regime of 30 °C-950 °C in air atmosphere with a flow rate of 60 mL/min.

3 Results and discussion

3.1 Thermodynamics characteristics analysis

Thermodynamics characteristics analysis can contribute to exploring the thermal behavior of vanadium slag during microwave oxidation roasting process. Referring to the elemental compositions of vanadium slag (Table 1), the slag sample contained high content of oxygen (O) element and various transition metal elements, mainly including Fe, Mn, V, Cr, and Ti elements. Therefore, as long as oxygen (O_2) content is sufficient in the roasting environment and the required thermodynamic conditions for those oxidation reactions are reached, the oxidation reactions of those transition metal elements will occur during microwave oxidation roasting process. In addition, referring to the phase compositions of vanadium slag (Fig. 1(a)), the main metal elements existed in the phase form of (Mn, Fe)(V, Cr)$_2O_4$, (Mn, Fe)$_2SiO_4$ and Fe_2TiO_4; hence, it could be concluded that iron (Fe) mainly existed as ferrous iron (Fe^{2+}), manganese (Mn) mainly existed as manganous iron (Mn^{2+}), the main valence states of vanadium (V) and chromium (Cr) were both in trivalent iron, namely V^{3+} and Cr^{3+}, respectively, and titanium (Ti) mainly existed in the form of tetravalent titanium iron (Ti^{4+}). From the above analysis about the main metal elements in the vanadium slag and the corresponding main valence states, the oxidation reactions probably appeared in the vanadium slag were presented in Table 2, meanwhile the corresponding dependency of standard Gibbs free energy (ΔG^{θ}) on temperatures for those oxidation reactions was plotted in Fig. 4, wherein Fig. 4(a) and Fig. 4(b) corresponded to the first 7 reactions and the last 6 reactions numbered in Table 2, respectively, and the thermodynamic data were obtained by FactSage thermodynamic software.

Summarized from Table 2, it could be understood that the vanadium slag contains these phase conversions during microwave oxidation roasting process: $FeO \rightarrow Fe_3O_4 \rightarrow Fe_2O_3$, $MnO \rightarrow Mn_3O_4 \rightarrow Mn_2O_3 \rightarrow MnO_2$, $V_2O_3 \rightarrow VO_2 \rightarrow V_2O_5$, $Cr_2O_3 \rightarrow CrO_2 \rightarrow CrO_3$, and $TiO \rightarrow Ti_2O_3 \rightarrow TiO_2$, according to the step-by-step conversion principle of metal oxides (Gao and Jiang, 2018; Li et al., 2019a; Li et al., 2019b; Zhang and Liu, 2016). Additionally, it can be observed from Fig. 4 that the dependence of ΔG^{θ} for the oxidation reactions of metal oxides in vanadium slag on temperature all presented an increasing trend, denoting that the improvement of roasting temperature was not conducive to the progress of those oxidation reactions, complying with the second law of thermodynamics. With roasting temperature increasing, those oxidation reactions will proceed more and more slowly and to a lesser extent. In detail, at temperatures higher than 93.1 °C, the oxidation reaction of $2Cr_2O_3(s)+O_2(g)=4CrO_2(s)$ will become difficult and finally be prohibited, and the oxidation reaction of $2CrO_2(s)+O_2(g)=2CrO_3(s)$ will hardly occur; therefore, at the considered temperature regime of room temperature to 950 °C in the present study, chromium (Cr) will still exist in the trivalent state (Cr^{3+}) after finishing the microwave oxidation roasting process of vanadium slag. Similarly, at temperatures exceeding 529.0 °C, the oxidation reaction of $2Mn_2O_3(s)+O_2(g)=4MnO_2(s)$ will become difficult and finally be prohibited; therefore, at the considered temperature regime of room temperature to 950 °C, manganese (Mn) will exist mainly in the form of Mn_3O_4 and Mn_2O_3 phases. Meanwhile, through the same analysis based on Fig. 4, at the considered temperature regime of room temperature to 950 °C, iron (Fe) could be considered to exist mainly in Fe_3O_4 and Fe_2O_3 phases, vanadium (V) will exist mainly in the form of VO_2 and V_2O_5 phases, and titanium (Ti) will still exist in the tetravalent

state (Ti^{4+}). Moreover, carbon (C) element will also react with oxygen (O_2), sharing and consuming some oxygen (O_2) in the roasting environment. Therefore, the complete and incomplete oxidation reactions of carbon (C) element will provide some degree of inhibition and competition for other oxidation reactions of metal elements with oxygen (O_2). And it can be observed from Fig. 4 that the dependency of ΔG^{θ} on temperatures for the oxidation reaction of carbon (C) element presented a decreasing trend, indicating that improving temperature was beneficial to the oxidation reaction of carbon (C) element, hence the degree of inhibition and competition originated from carbon (C) element will become more obvious and intense.

3.2 Thermogravimetric characteristics analysis

Thermogravimetric characteristics analysis can reveal the thermochemical characteristics of vanadium slag, further assisting to explore the relationship between the microwave absorption properties and thermal behavior in the microwave field. Therefore, thermogravimetric measurements for vanadium slag were conducted at different heating rates, and the obtained curves were depicted in Fig. 5.

Fig. 5(a) presented the TG curves. From Fig. 5(a), three TG curves were observed to present the similar trend with temperature for the weight change of vanadium slag, and the thermochemical characteristics of vanadium slag could be considered to be composed by three stages divided by temperatures: (1) the first stage (30 °C to 280 °C), was assigned to the dehydration stage. Although the vanadium slag was dried at 105 °C for 12 h before testing, there also existed a certain amount of adsorption water and bound water in the tested vanadium slag sample; therefore, adsorption water and bound water will escape from slag

sample at this stage. Moreover, with temperature rising from 30 °C to 280 °C, the weight of slag sample firstly went down, and then went up slightly, finally fluctuated repeatedly. The weight change at the temperature regime was attributed to the result of superimposing the two processes: the removal of surface water and bound water, and the partial slow oxidation reactions of free metal oxides, mainly divalent metal oxides (FeO and MnO) and a bit of trivalent metal oxide (V_2O_3 and Cr_2O_3), which was not wrapped and bound in the spinel phase (i.e. (Mn, Fe)(V, Cr)$_2O_4$) and olivine phase (i.e. (Mn, Fe)$_2SiO_4$). Wherein the removal of surface water and bound water rendered a decrease in weight, the partial slow oxidation reactions of metal oxides rendered an increase in weight, presenting a weight loss on the whole. The overall weight loss of vanadium slag at this stage was 0.924%, 0.707%, and 0.847%, with the heating rate improving from 10 °C/min to 30 °C/min. (2) The second stage (280 °C 650 °C), the significant weight gain at this stage was caused by the oxidation decomposition of olivine phase and normal spinel phase. Wherein olivine phase was decomposed and oxidized into Mn_2SiO_4 and Fe_2SiO_4 phases at 300 °C, followed by Fe^{2+} and Mn^{2+} irons existed in the decomposed products of olivine phase were completely oxidized into the corresponding high-valence metal oxides and quartz phase at 600 °C (Li et al., 2011; Zhang and Liu, 2016), including Fe_3O_4, Fe_2O_3, Mn_3O_4, Mn_2O_3, MnO_2, and SiO_2, which rendered the great weight increment for vanadium slag. In addition, normal spinel phase started to be decomposed into FeV_2O_4, MnV_2O_4, $FeCr_2O_4$, and $MnCr_2O_4$ phases at temperatures in excess of 500 °C, and the decomposed products of normal spinel phase were oxidized into inverse spinel phase (i.e. Fe_2VO_4 and Fe_2CrO_4) at about 600 °C and completely decomposed and oxidized at temperature lower than 700 °C, accompanying with small

amount of Fe_2O_3, $(Fe_{0.6}, Cr_{0.4})_2O_3$, Fe_2TiO_5 phases, which also contributed to the weight gain of vanadium slag to some extent (Gao and Jiang, 2018; Zhang and Liu, 2016). The weight gain of vanadium slag at this stage was 3.416%, 0.759% and 1.610% with the heating rate improved from 10 °C/min to 30 °C/min. (3) The third stage (650 °C-950 °C), was the oxidation decomposition of vanadium chromium spinel, accompanying by the weight gain of vanadium slag with 5.592%, 4.668% and 5.248% as the heating rate improved from 10 °C/min to 30 °C/min. Concluded from the above thermodynamics characteristics analysis, chromium (Cr) will still exist in the trivalent state (Cr^{3+}) in the vanadium slag at the measured temperature regime. Therefore, this thermodynamic characteristics of vanadium slag were mainly represented by the oxidization process of V^{3+} irons in vanadium chromium spinel into V^{4+} and V^{5+} irons, followed by the V^{4+} and V^{5+} irons were conjugated with Fe^{3+}, Mn^{2+} and Ca^{2+} irons to form acid soluble vanadate, including $Mn_2V_2O_7$, $FeVO_4$, $CaVO_3$, CaV_2O_7, $CrVO_4$, and $Cr_{0.07}V_{1.93}O_4$ (Gao and Jiang, 2018; Zhang and Liu, 2016).

Fig. 5(b) displayed the DTG curves. The same phenomenon was observed from Fig. 5(b), referring to the three DTG curves displayed the similar changing trend with temperature, with one exothermic peak at the first stage, three exothermic peaks at the second stage, and one exothermic peak and two endothermic peaks at the third stage. During the first stage, the exothermic peak was ascribed to the partial slow oxidation reactions of free metal oxides, at 104.9 °C, 104.9 °C and 134.6 °C with the heating rate improved from 10 °C/min to 30 °C/min. During the second stage, the three exothermic peaks at near 520 °C, 580 °C and 610 °C, were assigned to the oxidation decomposition of olivine phase and normal spinel phase (Zhang and Liu, 2016). During the third stage, the two endothermic peaks at near 760 °C and 820 °C were

attributed to the melt of vanadate generated by the oxidation decomposition of vanadium chromium spinel, and the exothermic peak at near 860 °C was assigned to the oxidation decomposition of vanadium chromium spinel (Zhang and Liu, 2016).

Fig. 5(c) showed the DSC curves. From Fig. 5(c), the same phenomenon as the DTG curves trend with temperature can also observed, with two epitaxial termination temperature peaks. The epitaxial termination temperature peak implies the intersection of the maximum weight loss line and the tangent of the DSC curve, indicating the maximum weight loss of vanadium slag occurred at the temperature. Wherein the first peak was attributed to the partial slow oxidation reactions of free metal oxides, at 80.18 °C, 131.59 °C and 154.91 °C with the heating rate improved from 10 °C/min to 30 °C/min; and the second peak was assigned to the oxidation decomposition of vanadium chromium spinel, at 804.87 °C, 807.96 °C and 835.09 °C as the heating rate improved from 10 °C/min to 30 °C/min. The two peaks were both exothermic peak.

3.3 Dielectric properties analysis

The dielectric properties of vanadium slag were measured at 2450 MHz, including the dielectric constant (ε_r'), dielectric loss factor (ε_r''), and loss tangent coefficient (tan δ). The obtained results were depicted in Fig. 6.

3.3.1 Dielectric constants analysis

Fig. 6(a) illustrated the dielectric constant (ε_r') of vanadium slag. ε_r' denotes the ability of the material to absorb and store microwave energy (Li et al., 2020d; Ye at al., 2019). From Fig. 6(a), the ε_r' value of vanadium slag was determined with 34.447 (F/M) at room temperature, indicating the vanadium slag endows excellent microwave absorption properties.

The high ε_r' value was attributed to that the vanadium slag contained a wide variety of metal elements and metal oxides (referred to Table 1 and Fig. 1), which both show strong responsiveness to microwaves (He et al., 2019; Li et al., 2020d). As temperature improved to 500 °C, the ε_r' value presented a slow increasing trend with temperature rising, with the initial value of 34.447 (F/M) gradually increased to 52.677 (F/M). The increase of ε_r' value at this temperature regime (room temperature-500 °C) was attributed to the result of superimposing the influence of the two stages: the dehydration stage at the first stage and the oxidation decomposition of olivine phase at the second stage. Wherein the removal of surface water and bound water rendered a decrease of ε_r' value of vanadium slag, meanwhile the oxidation decomposition of olivine phase rendered an increase. It's well-known that water has strong microwave absorption properties; therefore, the dehydration of water in slag sample is bound to render a decrease to the microwave absorption properties of vanadium slag. On the other hand, olivine phase was decomposed into Mn_2SiO_4 and Fe_2SiO_4 phases and oxidized into Fe_2O_3 and SiO_2 at 300 °C, and then Fe^{2+} and Mn^{2+} irons existed in the decomposed products of olivine phase were gradually oxidized into the corresponding high-valence metal oxides, such as Fe_3O_4, Fe_2O_3, Mn_3O_4, Mn_2O_3, and MnO_2 (Li et al., 2011; Zhang and Liu, 2016). Wherein the order of the microwave absorption properties of different oxides of the same metal is as following: $Fe_2O_3 > Fe_3O_4 > FeO$, and $MnO_2 > Mn_2O_3 > Mn_3O_4 > MnO$ (He et al., 2019; Su et al., 2015); therefore, the oxidation reactions of low-valence metal oxides caused an increment in ε_r' value of vanadium slag. Under the combined influence of the two processes, the ε_r' value presented a slow increasing trend on the whole. Meanwhile, once temperature exceeding 500 °C, the ε_r' value suddenly rose to a much higher value, with

52.677 (F/M) moved up to 117.959 (F/M) at 550 °C; and with temperature continually improving to 850 °C, there was absent of significant change for ε_r' value of vanadium slag. The reason for the phenomenon was consistent with the above analysis for thermogravimetric characteristics. The normal spinel phase started to be decomposed into FeV_2O_4, MnV_2O_4, $FeCr_2O_4$ and $MnCr_2O_4$ phases at temperatures in excess of 500 °C, and the decomposed products of normal spinel phase were oxidized into inverse spinel phase (i.e. Fe_2VO_4 and Fe_2CrO_4), accompanying with Fe_2O_3, $(Fe_{0.6}, Cr_{0.4})_2O_3$ and Fe_2TiO_5 phases, rendering the sharp increase of ε_r' value at this short temperature range (Gao and Jiang, 2018; Zhang and Liu, 2016). Additionally, at temperature higher than 550 °C, in the one hand, normal spinel phase was decomposed into FeV_2O_4, MnV_2O_4, $FeCr_2O_4$, and $MnCr_2O_4$ phases, followed by the decomposed products were oxidized into inverse spinel phase (i.e. Fe_2VO_4 and Fe_2CrO_4) at about 600 °C and completely decomposed and oxidized at temperature lower than 700 °C, providing Fe^{3+}, Mn^{2+} and V^{3+} irons (Gao and Jiang, 2018; Zhang and Liu, 2016); on the other hand, the V^{3+} irons in vanadium chromium spinel was oxidized into V^{4+} and V^{5+} irons, and followed by the V^{4+} and V^{5+} irons were conjugated with Fe^{3+}, Mn^{2+} and Ca^{2+} irons to form acid soluble vanadate, such as $Mn_2V_2O_7$, $FeVO_4$, $CaVO_3$, CaV_2O_7, $CrVO_4$, and $Cr_{0.07}V_{1.93}O_4$ (Gao and Jiang, 2018; Zhang and Liu, 2016), consuming the content of Fe^{3+}, Mn^{2+} and V^{3+} irons and further to render the changing trend of ε_r' value at this temperature range.

3.3.2 Dielectric loss factors analysis

Fig. 6(b) illustrated the dielectric loss factor (ε_r'') of vanadium slag. ε_r'' indicates the ability of the substance to convert the absorbed microwave energy into internal energy. Moreover, the three values, ε_r', ε_r'' and tan δ are relational, thus the third value can be

determined by the other two values (Li et al., 2020d; Ye at al., 2019). Therefore, the reasons mentioned in the analysis for the dielectric constant (ε_r') changing with temperature are also suitable to be utilized to the analysis of dielectric loss factor (ε_r''). As demonstrated in Fig. 6(b), the ε_r'' value was determined with a high value of 1.47 (F/M) at room temperature, and then improved to 2.10 (F/M) at 100 °C, next slightly dropped to 1.90 (F/M) at 500 °C, followed by it suddenly dropped to 1.35 (F/M) at 550 °C, finally it presented no significant change with temperature rising to 850 °C, accompanying a similar value of 1.35(F/M). The temperature points for the significant change of ε_r'' value at 500 °C and 550 °C were the same as the emphasized temperature points appeared in the ε_r' curve.

3.3.3 Loss tangent coefficients analysis

Fig. 6(c) illustrated the loss tangent coefficient (tan δ) of vanadium slag. tan δ represents the conversion efficiency of the substance related to the ε_r'' value (Li et al., 2020d; Ye at al., 2019). As depicted in Fig. 6(c), the tan δ curve presented the same changing trend with the ε_r'' curve. The tan δ value was determined at 0.0430 at room temperature, and improved to 0.0597 at 100 °C, and then slightly dropped to 0.0361 at 500 °C, followed by it suddenly dropped to 0.0114 at 550 °C, finally it presented no significant change with temperature rising to 850 °C, accompanying by a value of 0.0116. The temperature points for the significant change of tan δ value were the same as the emphasized temperature points marked in the ε_r' curve and ε_r'' curve, appeared at 100 °C, 500 °C and 550 °C.

3.4 Microwave heating characteristics analysis

Microwave heating characteristics of vanadium slag were measured at 2450 MHz with different microwave powers, further to assess the correctness and rationality of dielectric

properties analysis, and the results were plotted in Fig. 7.

As depicted in Fig. 7, for the same final target temperature at near 950 °C, it took 14.0 min for vanadium slag to be heated from room temperature to the target temperature under a microwave irradiation of 600 W, meanwhile with 10.0 min at 800 W, 7.0 min at 1000 W, and 7.0 min at 1200 W, respectively. It's worth noticing the heating time under 1000 W and 1200 W was the same, both are 7.0 min, but the final reached temperatures of vanadium slag were different, with 950 °C under 1000 W and 957 °C under 1200 W. In addition, as presented in Fig. 7, the microwave heating characteristics of vanadium slag could be considered to contain three processes divided by heating rates: the gradual rising process at the early stage, the maximum heating rate in the medium stage, and the gradual decreasing process in late stage. The change of microwave heating characteristics of vanadium slag was consistent with that of dielectric properties. As shown in Fig. 6(a), the changing trend of dielectric constant (ε_r') with temperature at the front section was much sharper than that at the middle section or the rear section, and the changing trend at the front section was bigger than that at the rear section. The changing trend of dielectric constant (ε_r') with temperature rendered the maximum heating rate appeared in the medium stage, and the heating rate at the front section was bigger than that at the rear section. As shown in Fig. 7, the heating rate at the front and the rear section was 24 °C/min and 20 °C/min under 600 W, with 58 °C/min and 12 °C/min under 800 W, 42 °C/min and 48 °C/min under 1000 W, and 78 °C/min and 26 °C/min under 1200 W, respectively. Meanwhile, the highest heating rates were determined with 185 °C/min at 427 °C under 600 W, 180 °C/min at 490 °C under 800 W, 250 °C/min at 553 °C under 1000 W, and 233 °C/min at 507 °C under 1200 W, respectively. The short heating times and the

high heating rates claimed that the vanadium slag showed strong responsiveness to microwaves and endowed excellent microwave absorption properties. Moreover, the highest heating rates under different microwave powers appeared at the temperature regime of 500 °C to 550 °C, which the temperature range also roughly matched the temperature range for the appearance of the maximum dielectric constant appeared. The maximum dielectric constant and highest microwave heating rate of vanadium slag both appeared at 500 °C to 550 °C, which is also the main temperature regime of the oxidation decomposition of olivine phase and normal spinel phase, suggesting the appropriate process temperature for microwave heating technology to recycle vanadium slag. On the basis of the above analysis for microwave heating characteristics, it can be claimed that that the dielectric properties of vanadium slag were numerically correct, and the corresponding analysis was rational.

3.5 Phase structure characterization analysis

The vanadium slag sample after microwave oxidization roasting at 950 °C was determined by XRD and FT-IR characterization, expecting to reveal the oxidation decomposition behavior of vanadium slag and further to contribute to verifying the analysis for the thermal behavior of vanadium slag in the microwave field. The corresponding XRD pattern and FT-IR spectra were illustrated as Fig. 8.

3.5.1 XRD characterization analysis

For the phase compositions of the microwave roasted slag sample, it was observed from Fig. 8(a) that the main phases included $FeCr_2O_4$ phase (JCPDS: 34-0140), Fe_2SiO_4 phase (JCPDS: 34-0178), Fe_3O_4 phase (JCPDS: 19-0629), Fe_2O_3 phase (JCPDS: 39-1346), and Mn_3O_4 phase (JCPDS: 13-0162), with small amount of VO_2 phase (JCPDS: 43-1051), V_2O_5

phase (JCPDS: 41-1426), and SiO_2 phase (JCPDS: 46-1045). Compared with the raw slag sample (Fig. 1(a)), it can be observed from Fig. 8(a) that the diffraction peaks of normal spinel phase and olivine phase disappeared, substituted by the appearance of the diffraction peaks of new phases, such as $FeCr_2O_4$, Fe_2SiO_4, Mn_3O_4, VO_2, and V_2O_5. Wherein $FeCr_2O_4$ phase was formed by the decomposition of normal spinel phase, Fe_2SiO_4 phase was formed by the decomposition of olivine phase, Mn_3O_4 phase was formed by the oxidization of the decomposed products of normal spinel phase, VO_2 and V_2O_5 phases were formed by the oxidation decomposition of vanadium chromium spinel. Moreover, the intensities of the diffraction peaks of Fe_2O_3 phase became higher, which was attributed to that some new Fe_2O_3 phase was generated by the oxidation decomposition of normal spinel phase.

3.5.2 FT-IR characterization analysis

For the chemical functional groups of the roasted slag sample, it was presented as Fig. 8(b) that the FT-IR absorption bands appeared at 472.57 cm^{-1}, 572.48 cm^{-1}, 820.75 cm^{-1}, 876.86 cm^{-1}, 916.97 cm^{-1}, 953.59 cm^{-1}, 1090.44 cm^{-1}, 1636.90 cm^{-1}, 2360.47 cm^{-1}, and 3457.60 cm^{-1}. Compared with the raw slag sample (Fig. 1(b)), it can be observed from Fig. 8(b) that after microwave oxidation roasting, the absorption bands at 468.09 cm^{-1} and 578.52 cm^{-1} in the raw slag shifted to 472.57 cm^{-1} and 572.48 cm^{-1} in the roasted slag, respectively, which was attributed to the oxidation decomposition of normal spinel phase into inverse spinel phase (Hoex et al., 2006; Ishii and Nakahira, 1972; Zhang and Liu, 2016). Similarly, the absorption bands at 876.59 cm^{-1} and 962.88 cm^{-1} in the raw slag shifted to 876.86 cm^{-1} and 953.59 cm^{-1} in the roasted slag, respectively, which was ascribed to the oxidation decomposition of olivine phase (Jeanloz, 1980; Zhang and Liu, 2016). The absorption bands

at 820.75 cm^{-1} and 916.97 cm^{-1} were assigned to the stretching vibrations of VO_4 group (Bencic et al., 2000; Morton et al., 2010; Vuk et al., 2001), originating from the oxidation decomposition of vanadium chromium spinel. The absorption band at 1090.44 cm^{-1} was assigned to the Si-O asymmetric stretching vibrations, resulting from the oxidation decomposition of olivine phase (Hu et al., 2003; Liu et al., 2011; Wang et al., 2014). Additionally, the absorption bands at 1636.90 cm^{-1}, 2360.47 cm^{-1} and 3457.60 cm^{-1} were caused by the bending and stretching vibrations of -OH bond of surface water molecules (Chen et al., 2014; Mostafa et al., 2009); meanwhile, combining with Fig. 1(b) and Fig. 8(b), those bands in the roasted slag were stronger and deeper than those corresponding bands in the raw slag, implying that microwave heating can enhance the adsorbent ability of vanadium slag. The finding was consistent with the dielectric properties analysis, corresponded to that the dielectric constant of the roasted slag was much higher than the raw slag.

4 Conclusions

Recycling vanadium slag with high contents of vanadium (V) and chromium (Cr) can significantly reduce waste of resources and environmental hazard, and microwave heating instead of conventional methods performs sound application prospects. In this study, the microwave absorption properties of vanadium slag were determined, and the thermal behavior of vanadium slag was investigated to reveal the relation between microwave absorption properties and temperature. The main conclusions were drawn as following:

(1) The thermal behavior of vanadium slag were composed by three processes: the dehydration stage (30 °C-280 °C), the oxidation decomposition of olivine phase and normal spinel phase (280 °C-650 °C), and the oxidation decomposition of vanadium chromium spinel

(650 °C-950 °C). And the findings obtained from TG, XRD and FT-IR analysis were all matched.

(2) Vanadium slag endowed excellent dielectric properties, with the minimum ε_r' value of 34.447 (F/M) at room temperature gradually rose until temperature at 500 °C, the sharp increase stopped at temperatures exceeding 550 °C and kept balanced at near 117.959 (F/M). Meanwhile, the changing trend of dielectric properties with temperature corresponded to the three processes of the thermal behavior, with thermogravimetric characteristics analysis and the dielectric properties analysis matched.

(3) The microwave heating characteristics of vanadium slag can be divided into three processes attributed to the dielectric properties change: the gradual rising process at the early stage, the maximum heating rate at 500 °C to 550 °C, and the gradual decreasing process in late period. It took only 7.0 min for vanadium slag to be heated from 18 °C to 950 °C, with a highest heating rate of 250 °C/min. The short heating time and high heating rate claimed that the vanadium slag showed excellent responsiveness to microwaves, which the finding was consistent with the dielectric properties analysis.

The microwave absorption properties and thermal behavior of vanadium slag presented in the work can provide a valuable basic theoretical support for the further applications of processing vanadium slag by microwave heating.

Credit Author Statement

Prof. Guo Chen, Prof. Jin Chen and Prof. Jinhui Peng conceived and designed the study. Mr. Kangqiang Li, Miss Qi Jiang, Dr. Sivasankar Koppala, Dr. Mamdouh Omran and Prof. Guo Chen performed the experiments. Prof. Guo Chen and Prof. Jin Chen provided the raw materials. Prof. Jinhui Peng, Prof. Guo Chen and Dr. Lei Gao provided the microwave high temperature furnace. Mr. Kangqiang Li, Miss Qi Jiang and Prof. Jin Chen wrote the paper. Mr. Kangqiang Li, Dr. Mamdouh Omran, Dr. Sivasankar Koppala and Prof. Guo Chen reviewed and edited the manuscript. All authors read and approved the manuscript.

Declaration of interests

The authors declare that they have no known competing financial interests or personal relationships that could have appeared to influence the work reported in this paper.

Acknowledgments

The authors acknowledge the financial supports from the National Natural Science Foundation of China (No: U1802255, 51504110 and 51424114) and Innovative Research Team (in Science and Technology) in University of Yunnan Province were sincerely acknowledged.

Appendix A. Supplementary data

Supplementary material related to this article can be found in the online version.

References

[1] Abbas, S., Hwang, J., Kim, H., Chae, S.A., Kim, J.W., Mehboob, S., Ahn, A., Han, O.H., Ha, H.Y., 2019. An enzyme-inspired formulation of the electrolyte for stable and efficient vanadium redox flow battery at high temperatures. ACS. Appl. Mater. Inter. 11(30),

26842-26853. https://doi.org/10.1021/acsami.9b06790.

[2] Bencic, S., Orel, B., Surca, A., Stangar, U.L., 2000. Structural and electrochromic properties of nanosized Fe/V-oxide films with $FeVO_4$ and $Fe_2V_4O_{13}$ grains: comparative studies with crystalline V_2O_5. Sol. Energy. 68(6), 499-515. https://doi.org/10.1016/S0038-092X(00)00032-3.

[3] Chen, D.L., Liu, Z.S., Fan, B.B., Li, J., Cao, W.B., Wang, H.L., Lu, H.X., Xu, H.L., Zhang, R., 2014. Synthesis and characterization of TiN-coated cubic boron nitride powders. Int. J. Appl. Ceram. Technol. 11(5), 946-953. https://doi.org/10.1111/ijac.12080.

[4] Chen, G., Jiang, Q., Li, K.Q., He, A.X., Peng, J.H., Omran, M., Chen, J., 2020. Simultaneous removal of Cr(III) and V(V) and enhanced synthesis of high-grade rutile TiO_2 based on sodium carbonate decomposition. J. Hazard. Mater. 388, 122039. https://doi.org/10.1016/j.jhazmat.2020.122039.

[5] Chen, K.H., Peng, J.H., Srinivasakannan, C., Yin, S.H., Guo, S.H., Zhang, L.B., 2018. Effect of temperature on the preparation of yttrium oxide in microwave field. J. Alloy. Compd. 742, 13-19. https://doi.org/10.1016/j.jallcom.2018.01.258.

[6] Cheng, S., Chen, Q., Xia, H.Y., Zhang, L.B., Peng, J.H., Lin, G., Liao, X.F., Jiang, X., Zhang, Q., 2018. Microwave one-pot production of ZnO/Fe_3O_4/activated carbon composite for organic dye removal and the pyrolysis exhaust recycle. J. Clean. Prod. 188, 900-910. https://doi.org/10.1016/j.jclepro.2018.03.308.

[7] Gao, H.Y., Jiang, T., Xu, Y.Z., Wen, J., Xue, X.X., 2018. Change in phase, microstructure, and physical-chemistry properties of high chromium vanadium slag during microwave calcification-roasting process. Powder. Technol. 340, 520-527. https://doi.org/10.1016/j.powtec.2018.09.045.

[8] He, F., Chen, J., Chen, G., Peng, J.H., Srinivasakannan, C., Ruan, R., 2019. Microwave dielectric properties and reduction behavior of low-grade pyrolusite. JOM. 11, 3909-3914. https://doi.org/10.1007/s11837-019-03522-8.

[9] Hoex, B., Peeters, F.J.J., Creatore, M., Blauw, M.A., Kessels, W.M.M., Sanden V.M.C.M., 2006. High-rate plasma-deposited SiO_2 films for surface passivation of crystalline silicon. J. Vac. Sci. Technol. A. 24, 1823-1830. https://doi.org/10.1116/1.2232580.

[10] Hu, Q.L., Suzuki, H., Gao, H., Araki, H., Yang, W., Noda, T., 2003. High-frequency FTIR absorption of SiO_2/Si nanowires. Chem. Phys. Lett. 378, 299-304. https://doi.org/10.1016/j.cplett.2003.07.015.

[11] Ishii, M., Nakahira, M., Yamanata, J., 1972. Infrared absorption spectra and cation distributions in $(Mn, Fe)_3O_4$. Solid. State. Commun. 11, 209-212. https://doi.org/10.1016/0038-1098(72)91162-3.

[12] Jeanloz, R., 1980. Infrared spectra of olivine polymorphs: α, β phase and spinel. Phys. Chem. Miner. 5, 327-341. https://doi.org/10.1007/BF00307542.

[13] Li, H.Y., Long, H.L., Zhang, L.B., Yin, S.H., Li, S.W., Zhu, F., Xie, H.M., 2020. Effectiveness of microwave-assisted thermal treatment in the extraction of gold in cyanide tailings. J. Hazard. Mater. 384, 121456. https://doi.org/10.1016/j.jhazmat.2019.121456.

[14] Li, K.Q., Chen, G., Chen, J., Peng, J.H., Ruan, R., Srinivasakannan, C., 2019a. Microwave pyrolysis of walnut shell for reduction process of low-grade pyrolusite. Bioresource. Technol. 291, 121838. https://doi.org/10.1016/j.biortech.2019.121838.

[15]Li, K.Q., Chen, J., Chen, G., Peng,, J.H., Ruan, R., Srinivasakannan, C., 2019b. Microwave dielectric properties and thermochemical characteristics of the mixtures of walnut shell and manganese ore. Bioresource. Technol. 286, 121381. https://doi.org/10.1016/j.biortech.2019.121381.

[16]Li, K.Q., Chen, G., Li, X.T., Peng, J.H., Ruan, R., Omran, M., Chen, J., 2019c. High-temperature dielectric properties and pyrolysis reduction characteristics of different biomass-pyrolusite mixtures in microwave field. Bioresource. Technol. 294, 122217. https://doi.org/10.1016/j.biortech.2019.122217.

[17]Li, K.Q., Chen, J., Peng, J.H., Ruan, R., Srinivasakannan, C., Chen, G., 2020a. Pilot-scale study on enhanced carbothermal reduction of low-grade pyrolusite using microwave heating. Powder. Technol. 360, 846-854. https://doi.org/10.1016/j.powtec.2019.11.015.

[18]Li, K.Q., Jiang, Q., Chen, J., Peng, J.H., Li, X.P., Koppala, S., Omran, M., Chen, G., 2020b. The controlled preparation and stability mechanism of partially stabilized zirconia by microwave intensification. Ceram. Int. 46(6), 7523-7530. https://doi.org/10.1016/j.ceramint.2019.11.251.

[19]Li, K.Q., Chen, J., Peng, J.H., Koppala, S., Omran, M., Chen, G., 2020c. One-step preparation of CaO-doped partially stabilized zirconia from fused zirconia. Ceram. Int. 46(6), 6484-6490. https://doi.org/10.1016/j.ceramint.2019.11.129.

[20]Li, K.Q., Chen, J., Peng, J.H., Ruan, R., Orman, M., Chen, G., 2020d. Dielectric properties and thermal behavior of electrolytic manganese anode mud in microwave field. J. Hazard. Mater. 381, 121227. https://doi.org/10.1016/j.jhazmat.2019.121227.

[21]Li, W., Zheng, H.Y., Shen, F.M., 2019. Effect of roasting characteristics of

vanadium-rich slag on its vanadium leaching behavior. JOM. 71(9), 1-6. https://doi.org/10.1007/s11837-019-03578-6.

[22] Li, X.S., Xie, B., Wang, G.E., Li, X.J., 2011. Oxidation process of low-grade vanadium slag in presence of Na_2CO_3. T. Nonferr. Metal. Soc. 21(8), 1860-1867. https://doi.org/10.1016/S1003-6326(11)60942-4.

[23] Lin, G., Wang, S.X., Zhang, L.B., Hu, T., Cheng, S., Fu, L.K., Xiong, C., 2019. Enhanced and selective adsorption of Hg^{2+} to a trace level using trithiocyanuric acid-functionalized corn bract. Environ. Pollut. 244, 938-946. https://doi.org/10.1016/j.envpol.2018.08.054.

[24] Liu, J.W., Zhang, Q., Chen, X.W., Wang, J.H., 2011. Surface assembly of graphene oxide nanosheets on SiO_2 particles for the selective isolation of hemoglobin. Chem. Eur. J. 17, 4864-4870. https://doi.org/10.1002/chem.201003361.

[25] Liu, S.Y., Li, S.J., Wu, S., Wang, L.J., Chou, K.C., 2018. A novel method for vanadium slag comprehensive utilization to synthesize Zn-Mn ferrite and Fe-V-Cr alloy. J. Hazard. Mater. 354, 99-106. https://doi.org/10.1016/j.jhazmat.2018.04.061.

[26] Liu. S.Y., Wang, L.J., Chou, K.C., 2017. Selective chlorinated extraction of iron and manganese from vanadium slag and their application to hydrothermal synthesis of $MnFe_2O_4$. Acs. Sustain. Chem. Eng. 5(11), 10588-10596. https://doi.org/10.1021/acssuschemeng.7b02573.

[27] Morton, C.D., Slipper, I.J., Thomas, M.J.K., Alexander, B.D., 2010. Synthesis and characterisation of Fe-V-O thin film photoanodes. J. Photochem. Photobiol. A. 216, 209-214. https://doi.org/10.1016/j.jphotochem.2010.08.010.

[28] Mostafa, N.Y., Kishar, E.A., Abo-El-Enein, S.A., 2009. FTIR study and cation exchange capacity of Fe^{3+} and Mg^{2+} substituted calcium silicate hydrates. J. Alloy. Comp. 473, 538-542. https://doi.org/10.1016/j.jallcom.2008.06.029.

[29] Oldenburg, F., Nilsson, E., Schmidt, T.J., Gubler, L., 2019. Cover feature: tackling capacity fading in vanadium redox flow batteries with amphoteric polybenzimidazole/nafion bilayer membranes. ChemSusChem. 12(12), 2489-2489. https://doi.org/10.1002/cssc.201901508.

[30] Svoboda, R., Bulánek, R., Galusek, D., Hadidimasouleh, R., Ganjkhanlou, Y., 2018. Crystal formation in vanadium-doped zirconia ceramics. CrystEngComm, 20, 3105-3116. https://doi.org/10.1039/C8CE00538A.

[31] Su, X.J., Mo, Q.H., He, C.L., Ma, S.J., Que, S.J., 2015. Microwave absorption characteristics of manganese compounds. Min. Metal. Eng. 35(5), 90-94. https://doi.org/10.3969/j.issn.0253-6099.2015.05.024.

[32] Takahashi, J., Kawakami, K., Kobayashi, Y., 2018. Origin of hydrogen trapping site in vanadium carbide precipitation strengthening steel. Acta. Mater. 153, 193-204. https://doi.org/10.1016/j.actamat.2018.05.003.

[33] Teng, A.J., Xue, X.X., 2019. A novel roasting process to extract vanadium and chromium from high chromium vanadium slag using a NaOH-$NaNO_3$ binary system. J. Hazard. Mater. 379, 120805. https://doi.org/10.1016/j.jhazmat.2019.120805.

[34] Tian, L., Xu, Z.F., Chen, L.J., Liu, Y., Zhang, T.A., 2019. Effect of microwave heating on the pressure leaching of vanadium from converter slag. 184, 45-54. https://doi.org/10.1016/j.hydromet.2018.11.004.

[35] Vuk, A.S., Orel, B., Drazic, G., 2001. IR spectroelectrochemical studies of $Fe_2V_4O_{13}$, $FeVO_4$ and $InVO_4$ thin films obtained via sol-gel synthesis. J. Solid. State. Electr. 5, 437-449. https://doi.org/10.1007/s100080000183.

[36] Wang, P., Liu, H.Z., Niu, J.R., Li, R., Ma, J.T., 2014. Entangled Pd complexes over Fe_3O_4@SiO_2 as supported catalysts for hydrogenation and Suzuki reactions. Catal. Sci. Technol. 4, 1333-1339. https://doi.org/10.1039/C3CY00646H.

[37] Wang, Z.H., Zheng, S.L., Wang, S.N., Liu, B., Wang, D.W., Du, H., Zhang, Y., 2014. Research and prospect on extraction of vanadium from vanadium slag by liquid oxidation technologies. T. Nonferr. Metal. Soc. 24(5), 1273-1288. https://doi.org/10.1016/S1003-6326(14)63189-7.

[38] Wen, J., Jiang, T., Wang, J.P., Gao, H.Y., Lu, L.G., 2019. An efficient utilization of high chromium vanadium slag: Extraction of vanadium based on manganese carbonate roasting and detoxification processing of chromium-containing tailings. J. Hazard. Mater. 378, 120733. https://doi.org/10.1016/j.jhazmat.2019.06.010.

[39] Yang, Z.Y., Yi, H.H., Tang, X.L., Zhao, S.Z., Huang, Y.H., Xie, X.Z., Song, L.L., Zhang, Y.Y., 2019. Study of reaction mechanism based on further promotion of low temperature degradation of toluene using nano-CeO_2/Co_3O_4 under microwave radiation for cleaner production in spraying processing. J. Hazard. Mater. 373, 321-334. https://doi.org/10.1016/j.jhazmat.2019.03.062.

[40] Ye, X.L., Guo, S.H., Qu, W.W., Yang, L., Hu, T., Xu, S.M., Zhang, L.B., Liu, B.G., Zhang, Z.M., 2019. Microwave field: High temperature dielectric properties and heating characteristics of waste hydrodesulfurization catalysts, J. Hazard. Mater. 366, 432-438.

https://doi.org/10.1016/j.jhazmat.2018.12.024.

[41] Yin, Y., Wen, Z.H., Shi, L., Zhang, Z.Z., Yang, Z.F., Xu, C.L., Sun, H.Q., Wang, X.B., Yuan, A.H., 2019. Cuprous/vanadium sites on MIL-101 for selective CO adsorption from gas mixtures with superior stability. ACS. Sustain. Chem. Eng. 7(13), 11284-11292. https://doi.org/10.1021/acssuschemeng.9b00699.

[42] Zhao, Y.Z., Liu, B.G., Zhang, L.B., Guo, S.H., 2020. Microwave-absorbing properties of cathode material during reduction roasting for spent lithium-ion battery recycling. J. Hazard. Mater. 381, 121487. https://doi.org/10.1016/j.jhazmat.2019.121487.

[43] Zhang, X.F., Fang, D., Song, S.Z., Cheng, G.J., Xue, X.X., 2019. Selective leaching of vanadium over iron from vanadium slag. J. Hazard. Mater. 368, 300-307. https://doi.org/10.1016/j.jhazmat.2019.01.060.

[44] Zhang, X.F., Liu, F.G., Xue, X.X., Jiang, T., 2016. Effects of microwave and conventional blank roasting on oxidation behavior, microstructure and surface morphology of vanadium slag with high chromium content. J. Alloy. Compd. 686, 356-365. https://doi.org/10.1016/j.jallcom.2016.06.038.

[45] Zhang, G.Q., Zhang, T.A., Lu, G.Z., Zhang, Y., Liu, Y., Zhang, W.G., 2016. Effects of microwave roasting on the kinetics of extracting vanadium from vanadium slag. JOM. 68(2), 577-584. https://doi.org/10.1007/s11837-015-1736-6.

Table captions

Table 1 Chemical compositions of vanadium slag

Table 2 Oxidation reactions probably appeared in vanadium slag

Figure captions

Fig.1. XRD pattern (a) and FT-IR spectra (b) of raw vanadium slag

Fig.2. Schematic diagram of dielectric test system, (a) dielectric test device; (b) cylindrical resonant cavity in dielectric device

Fig.3. Schematic diagram of microwave furnace

Fig.4. Dependence of ΔG^{θ} for the oxidation reactions in vanadium slag on temperature

Fig.5. TG-DTG-DSC curves of vanadium slag, (a) TG curves; (b) DTG curves; (c) DSC curves

Fig.6. Dielectric properties of vanadium slag under microwave irradiation at 2450 MHz, (a) dielectric constant (ε_r'); (b) dielectric loss factor (ε_r''); (c) loss tangent coefficient (tan δ)

Fig.7. Microwave heating characteristics of vanadium slag at different microwave powers, (a) 600 W; (b) 800 W; (c) 1000 W; (d) 1200 W

Fig.8. XRD pattern (a) and FT-IR spectra (b) of the vanadium slag roasted at 950 °C

Table 1 Chemical compositions of vanadium slag

Compositions	C	O	Fe	Mn	V	Cr	Ti	Na
Mass/w%	1.62	37.1	27.4	5.24	7.37	1.38	5.98	0.519
Compositions	Mg	Al	Si	P	S	Cl	K	Ca
Mass/w%	2.22	2.48	6.67	0.0632	0.0818	0.0275	0.0892	1.69
Compositions	Zn	Ga	Sr	Zr	Nb	Others		
Mass/w%	0.0072	0.0087	0.0060	0.0104	0.0222	0.0148		

Table 2 Oxidation reactions probably appeared in vanadium slag

NO.	Reactions	NO.	Reactions
(1)	$6FeO(s)+O_2(g)=2Fe_3O_4(s)$	(8)	$2Cr_2O_3(s)+O_2(g)=4CrO_2(s)$
(2)	$4Fe_3O_4(s)+O_2(g)=6Fe_2O_3(s)$	(9)	$2CrO_2(s)+O_2(g)=2CrO_3(s)$
(3)	$6MnO(s)+O_2(g)=2Mn_3O_4(s)$	(10)	$4TiO(s)+O_2(g)=2Ti_2O_3(s)$
(4)	$4Mn_3O_4(s)+O_2(g)=6Mn_2O_3(s)$	(11)	$2Ti_2O_3(s)+O_2(g)=4TiO_2(s)$
(5)	$2Mn_2O_3(s)+O_2(g)=4MnO_2(s)$	(12)	$C(s)+O_2(g)=CO_2(g)$
(6)	$2V_2O_3(s)+O_2(g)=4VO_2(s)$	(13)	$2C(s)+O_2(g)=2CO(g)$
(7)	$4VO_2(s)+O_2(g)=2V_2O_5(s)$		

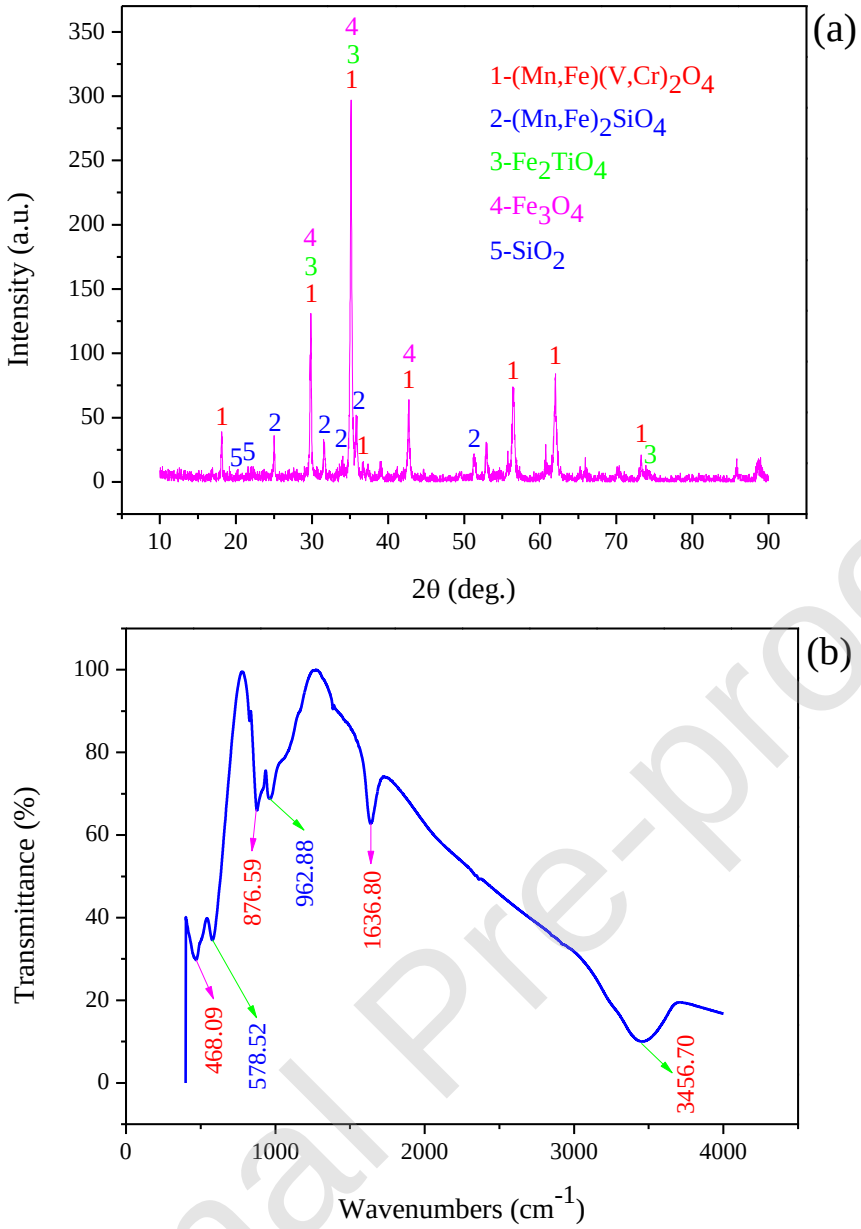

Fig.1. XRD pattern (a) and FT-IR spectra (b) of raw vanadium slag

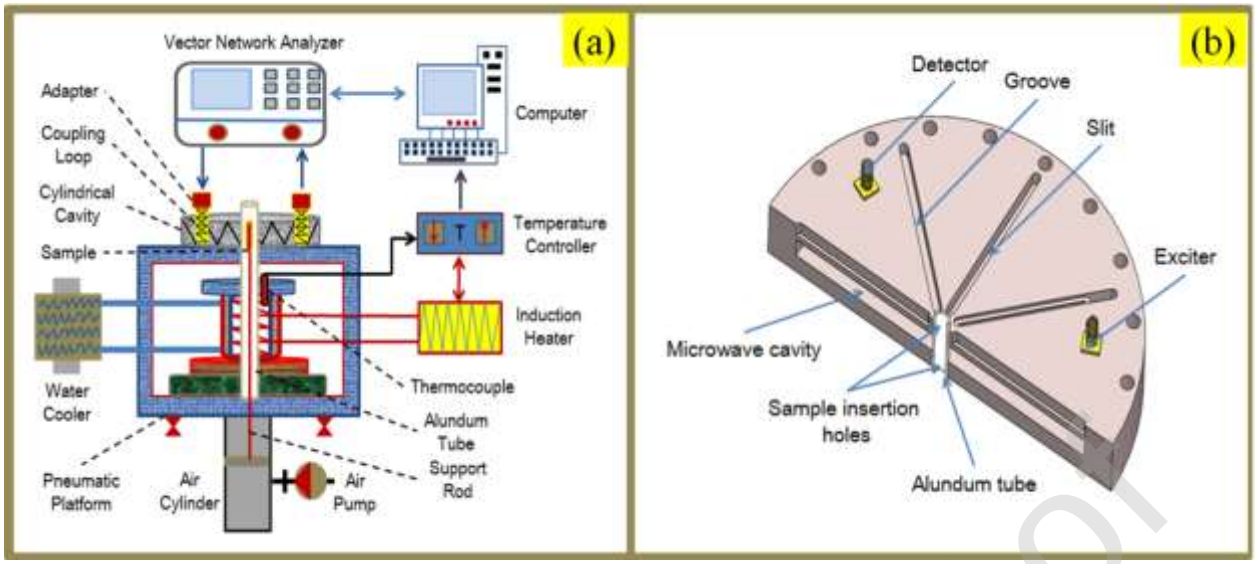

Fig.2. Schematic diagram of dielectric test system, (a) dielectric test device; (b) cylindrical resonant cavity in dielectric device

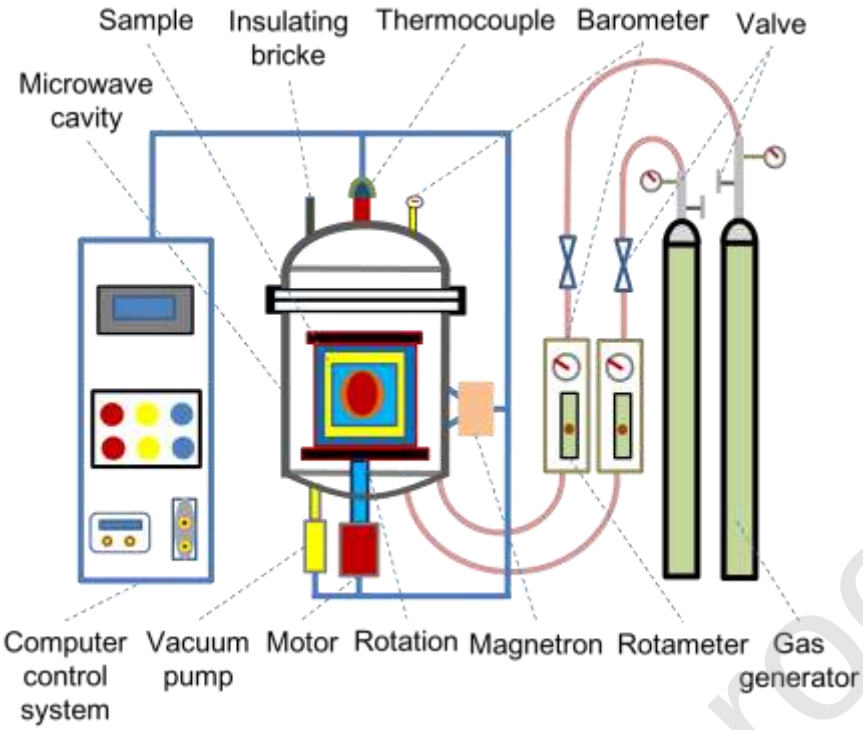

Fig.3. Schematic diagram of microwave furnace

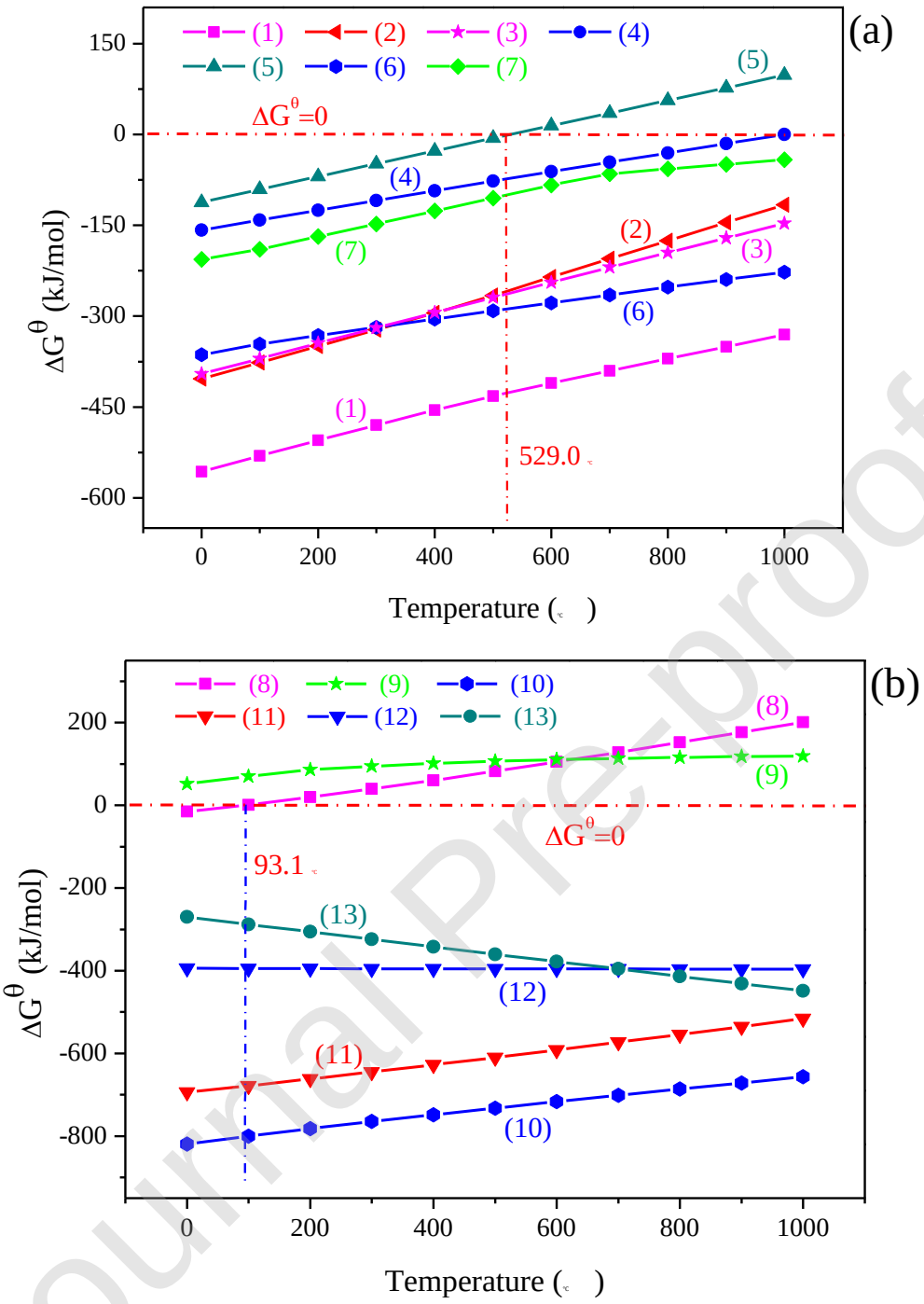

Fig.4. Dependence of ΔG^{θ} for the oxidation reactions in vanadium slag on temperature

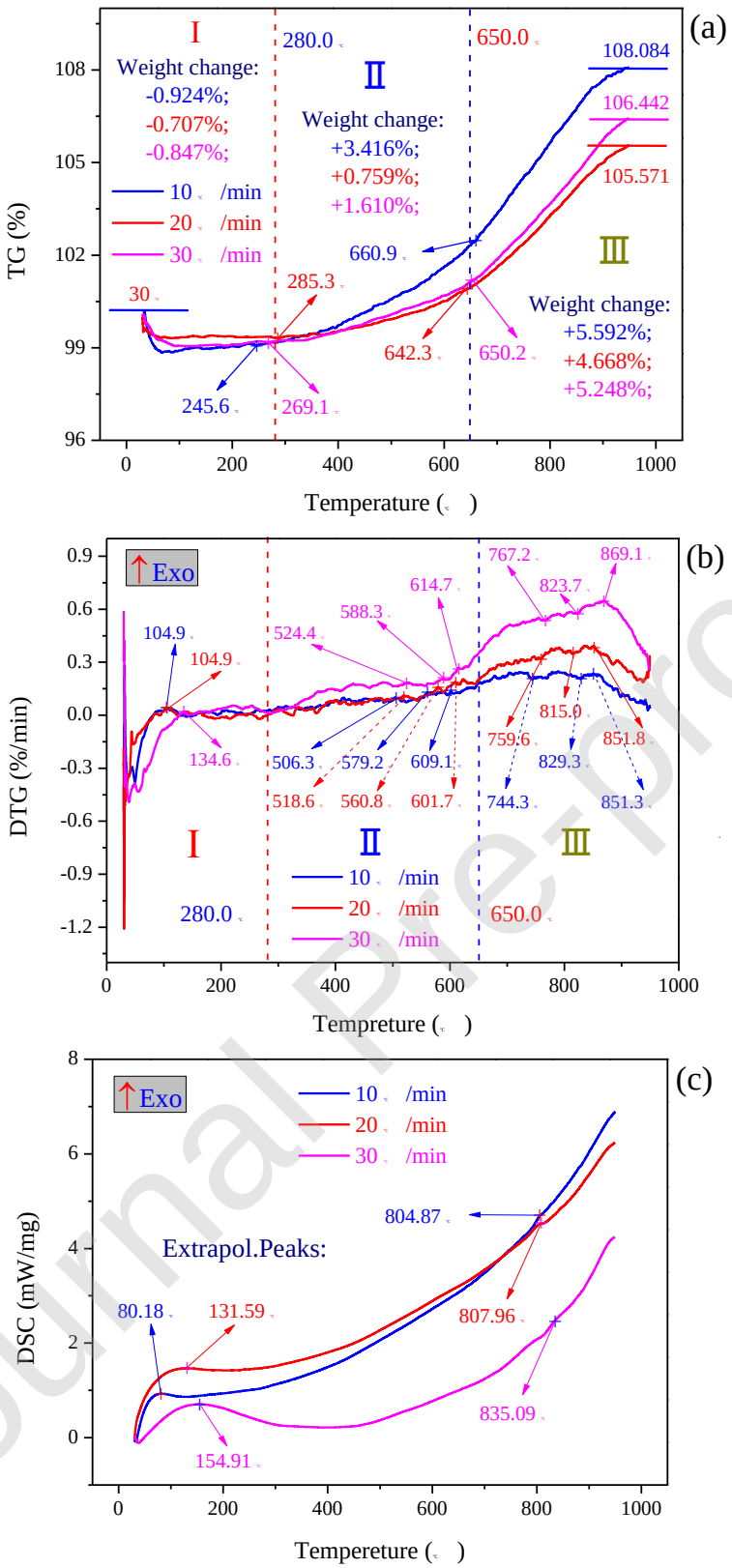

Fig.5. TG-DTG-DSC curves of vanadium slag, (a) TG curves; (b) DTG curves; (c) DSC curves

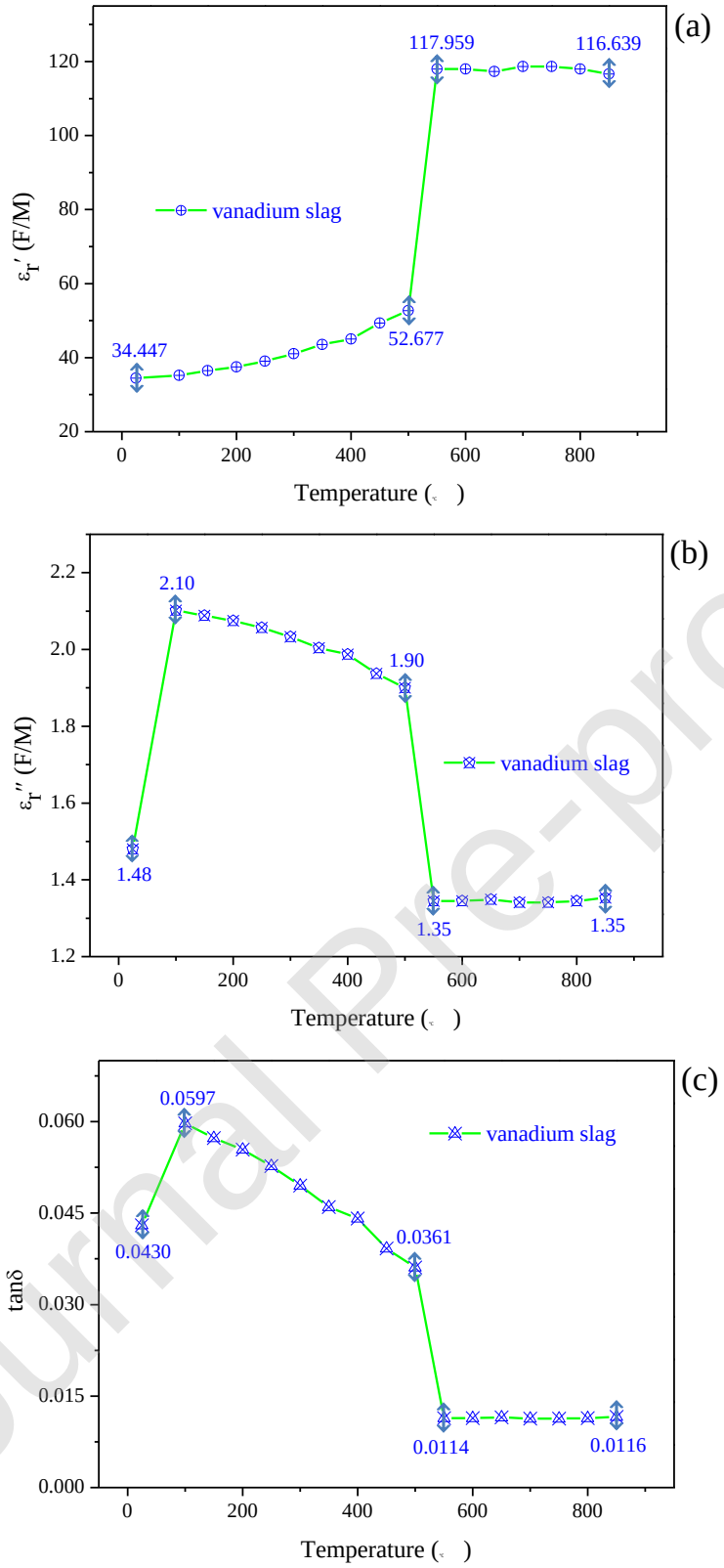

Fig.6. Dielectric properties of vanadium slag under microwave irradiation at 2450 MHz, (a) dielectric constant (ε_r'); (b) dielectric loss factor (ε_r''); (c) loss tangent coefficient (tan δ)

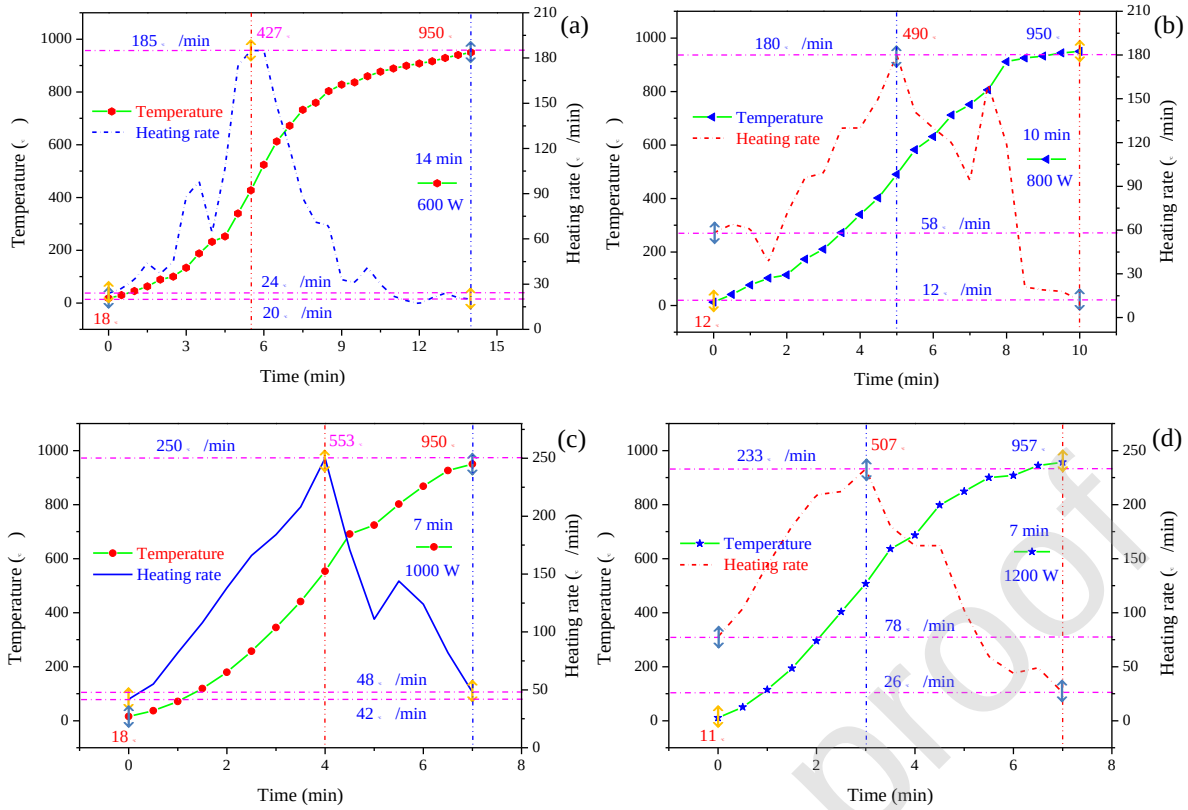

Fig.7. Microwave heating characteristics of vanadium slag at different microwave powers, (a) 600 W; (b) 800 W; (c) 1000 W; (d) 1200 W

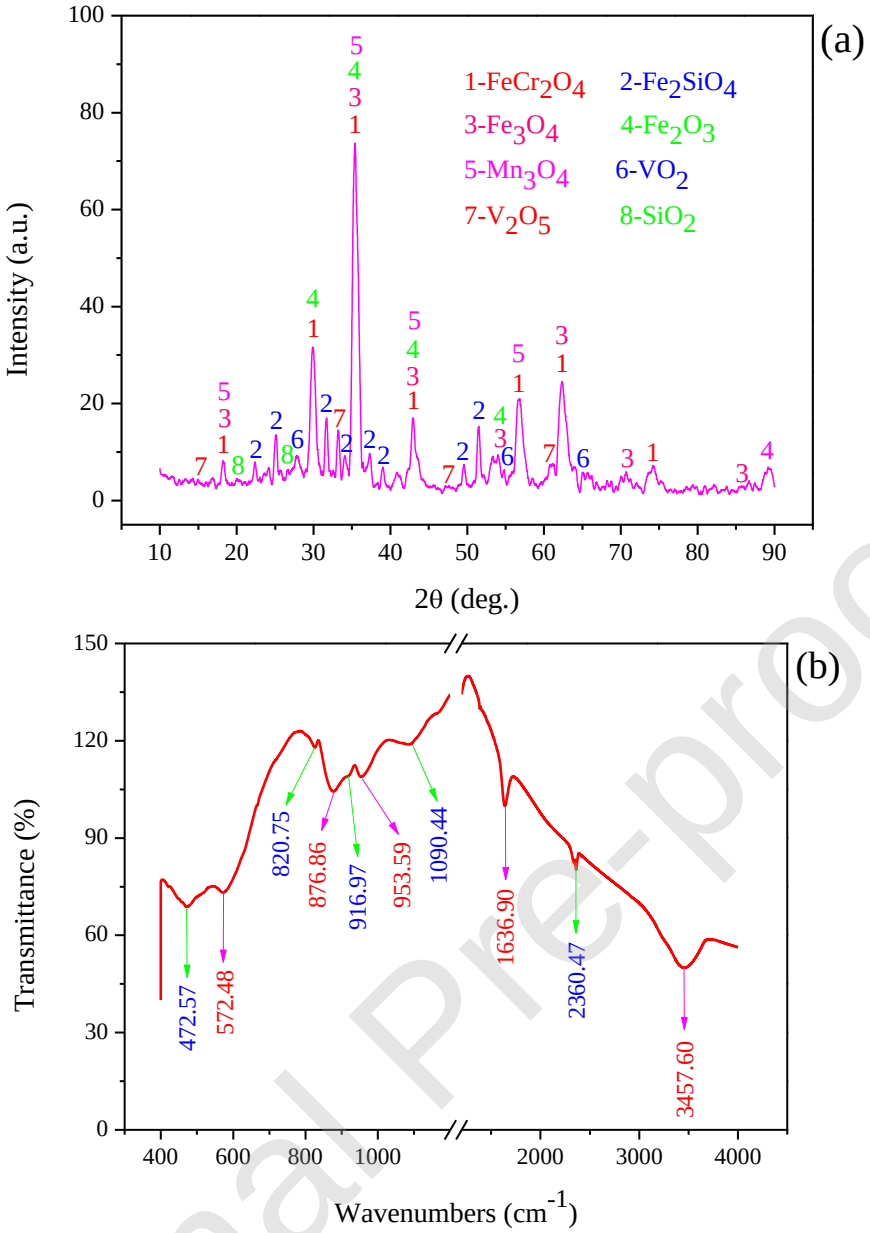

Fig.8. XRD pattern (a) and FT-IR spectra (b) of the vanadium slag roasted at 950 °C